Inorganic Chemistry

Article

pubs.acs.org/IC

Application of Atomic Hirshfeld Surface Analysis to Intermetallic Systems: Is Mn in Cubic $CeMnNi_4$ a Thermoelectric Rattler atom?

Mads R. V. Jørgensen,[†] Iben Skovsen,[†] Henrik F. Clausen,[†] Jian-Li Mi,[†] Mogens Christensen,[†] Eiji Nishibori,[‡] Mark A. Spackman,[§] and Bo B. Iversen*[,†]

[†]Center for Materials Crystallography, Department of Chemistry and iNANO, Aarhus University, Langelandsgade 140, DK-8000 Aarhus C, Denmark

[‡]Department of Applied Physics, Nagoya University, Nagoya 464-8603, Japan

[§]School of Biomedical, Biomolecular& Chemical Sciences, University of Western Australia, Crawley, Western Australia 6009, Australia

Supporting Information

ABSTRACT: The Mn atom in the cubic polymorph of $CeMnNi_4$ appears to be located in an oversized cage-like structure, and anomalously large atomic displacement parameters (ADPs) for the Mn atom indicate that it is a potential "rattler" atom. Here, multitemperature synchrotron powder X-ray diffraction data measured between 110 and 900 K are used to estimate ADPs for the Mn "guest" atom and the "host" structure atoms in cubic $CeMnNi_4$. The ADPs are subsequently fitted with Debye and Einstein models, giving Θ_D = 301(2) K for the "host" structure and Θ_E = 165(2) K for the Mn atom. This is higher than typical Einstein temperatures for rattlers in thermoelectric skutterudites and clathrates (Θ_E = 50−80 K), indicating that the Mn atom in cubic $CeMnNi_4$ is more strongly bonded. In order to probe the chemical interactions of the potential Mn rattler atom, atomic Hirshfeld surface (AHS) analysis is carried out and compared with AHS analysis of well-established guest atom rattlers in archetypical skutterudites, $MCoSb_3$. Surprisingly, the skutterudite rattlers have more deformed AHSs than the Mn atom in cubic $CeMnNi_4$. This is related to the highly ionic nature of the skutterudite rattlers, which is not taken into account in the neutral spherical atom approach of the AHS. Additionally, visualization of void spaces in the two materials using the procrystal electron density shows that while the Mn atom is tightly fitting in the $CeMnNi_4$ structure then the La atom in the skutterudite is truly situated in an oversized cage of the host structure. Overall, we conclude that the Mn atom in cubic $CeMnNi_4$ cannot be coined a rattler.

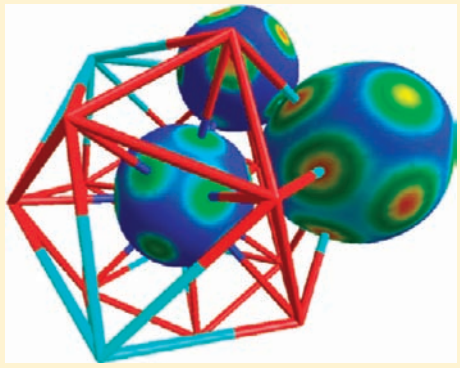

INTRODUCTION

Efficient use of our energy resources becomes more and more important as the world's energy supply continuously is being depleted and environmental concerns are pressing. Thermoelectric energy conversion is a promising technology for converting waste heat into useful electrical energy, and research in thermoelectric materials has increased significantly during the past decade.[1] This is also due to introduction of ground breaking new materials design concepts such as nanostructuring, lowering of materials dimensionality, and the concept of "phonon glass electron crystals (PGEC)".[2] The latter concept defines the hypothetical ideal thermoelectric material: a material which conducts electrical current like a crystal but heat like an amorphous glass.[2a] The thermoelectric efficiency of a material is given by the thermoelectric figure of merit $zT = S^2\sigma/\kappa$, where S is the Seebeck coefficient, σ is the electronic conductivity, and κ is the thermal conductivity, which consists of both an electronic (κ_e) and a lattice contribution (κ_l). Host−guest structures such as skutterudites ($M_xCo_4Sb_{12}$, where M often is a lanthanide atom) and clathrates ($M_8Ga_{16}Ge_{30}$, where M is a divalent cation) have been found to exhibit many of the features of a PGEC material.[3] These structures consist of host structures with large oversized cages in which guest atoms are trapped. The crystalline host structures have high power factors ($S^2\sigma$), and at the same time the guest atom contributes to lowering the thermal conductivity, thus leading to large values of zT. In these compounds a range of mechanisms lead to the observed low thermal conductivities, but it appears that the presence of loosely bonded guest atoms in oversized cages is one of the important contributors.[4] The guest atoms can, to a first approximation, be considered as independent Einstein oscillators, and due to the weak bonding with the host structure their vibrational energies are low and of similar magnitude to the acoustic phonons of the host structure. This in turn gives a possibility for the rattling guest atom motion to hybridize with the host structure vibrations, giving a strong reduction in the

Received: October 14, 2011
Published: January 20, 2012

   dx.doi.org/10.1021/ic202231k | *Inorg. Chem.* 2012, 51, 1916−1924

velocity and/or lifetime of the heat-carrying acoustic phonons, and thereby a significant reduction in the thermal conductivity.[4]

Rattling guest atoms are characterized by having large motion in the oversized cages, and this is observed as large atomic displacement parameters (ADPs) when the materials are studied with X-ray or neutron diffraction methods.[5] Indeed, early on Sales and co-workers suggested that the millions of ADPs deposited in crystal structure databases potentially could be used to search for new PGEC materials.[6] The present study concerns exactly such a case, namely, $CeMnNi_4$. In recent years this material has received increased attention due to potential application in spintronics.[7] There are two different polymorphs of $CeMnNi_4$, and the most investigated compound is the cubic phase belonging to the space group $F\bar{4}3m$ (Ce at 4*a*, Mn at 4*c*, and Ni at 16*e*, where $x \approx 5/8$),[7b] whereas the other polymorph belongs to the hexagonal space group $P6/mmm$.[8] The cubic phase has a fully ordered crystal structure, where the Mn atoms are located in large voids in the crystal structure, Figure 1.

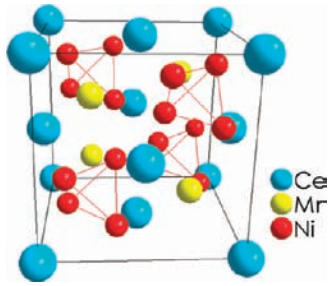

Figure 1. Crystal structure of the cubic polymorph of $CeMnNi_4$. Both Mn and a tetrahedron of Ni are located in one-eighth of the unit cell, indicating that Mn is placed in an oversized void.

Dhiman et al. established, based on powder neutron diffraction data, that these Mn atoms have large ADPs with values of 0.012(2) $Å^2$ at 90 K and 0.018(2) $Å^2$ at 300 K.[7b] For comparison Ni, which has a similar mass to Mn, has values of 0.004(1) $Å^2$ at 90 K and 0.009(2) $Å^2$ at 300 K. In the thermoelectric rattler structure of $La_{0.1}Co_4Sb_{12}$ the La ADPs are 0.007(1) $Å^2$ at 90 K and 0.018(2) $Å^2$ at 300 K, while the Co ADPs (similar in mass to Mn and Ni) are 0.00180(5) $Å^2$ at 90 K and 0.00393(7) $Å^2$ at 300 K.[9] Due to a range of systematic errors in common crystallographic data it is normally difficult to compare absolute values of ADPs between different studies.[10] Nevertheless, the Mn ADP in cubic $CeMnNi_4$ seems to have similar magnitude as the ADP of La in $La_{0.1}Co_4Sb_{12}$, and it is significantly larger than the ADPs of the other atoms in $CeMnNi_4$. Since $CeMnNi_4$ is a semimetal it was suggested that it could be a promising thermoelectric material.[7a]

In this paper we present crystal structure investigations of cubic $CeMnNi_4$ based on multitemperature synchrotron powder X-ray diffraction measurements. The Mn atom is confirmed to have a large ADP, but the estimated Einstein temperature is much higher than what is found in skutterudites and clathrates. To gain a better understanding of what constitutes a thermoelectric rattler, atomic Hirshfeld surface (AHS) analysis is used to probe the host–guest interactions both in cubic $CeMnNi_4$ and in the archetypical skutterudite structure where the rattling effect is well established.

EXPERIMENTAL SECTION

Synthesis. Hexagonal $CeMnNi_4$ was prepared by melting stoichiometric amounts of the elemental constituents (99.9 wt % purity Ce and Mn, 99.99 wt % purity Ni). The stoichiometric pure elements were placed in a water-cooled copper hearth and heated by high-frequency induction. The sample was remelted four times, and prior to melting the sample was cleaned in 2 M nitric acid and flipped to ensure a homogenization. The final ingot was hexagonal $CeMnNi_4$ (space group $P6/mmm$), confirmed by X-ray diffraction. The ingot was then heated in an evacuated quartz ampule at 1103 K for 35 days in order to obtain the cubic phase of $CeMnNi_4$.

Synchrotron Powder X-ray Diffraction. Part of the produced sample was ground and investigated by multitemperature, high-resolution synchrotron powder diffraction. The powder diffraction data were collected at beamline BL02B2, SPring8, Japan, using the large Debye–Scherrer camera.[11] A homogeneous grain size is important for measuring high-quality PXRD data. The powder was first floated with ethanol in a Petri dish and left for sedimentation. The top layer of the ethanol was removed into a new Petri dish and left for further sedimentation. The top layer was again removed into a new Petri dish, and the ethanol was evaporated, leaving a sample fraction of homogeneous grain size. The sample was transferred to a 0.2 mm quartz capillary and held in an ultrasound bath to obtain a dense packing of the powder. The synchrotron radiation wavelength was determined to be λ = 0.357469(8) Å using a CeO_2 standard (a = 5.411102 Å). For the data collected below room temperature, the temperature (110–300 K) was controlled using a cold nitrogen gas flow system. Data at elevated temperatures (300–900 K) were collected using a hot nitrogen gas flow system. The hot and cold systems are two separate systems.

The heat capacity (HC) was measured on a Quantum Design Physical Properties Measurement System (PPMS) using the HC option. In order to ensure good thermal contact between the sapphire shoe and the sample (mass = 37.246 mg) a known amount of N-grease was applied. The data were subsequently corrected for the N-grease contribution.

RESULTS AND DISCUSSION

Crystal Structure. The 31 individual data sets, measured at different temperatures, were Rietveld refined using the FULLPROF program.[12] Data above $2\theta = 61°$ were omitted in the refinements as the intensities could not be distinguished from the background. A pseudo-Voigt peak shape function with five parameters, one Gaussian, two Lorentzian, and two asymmetry parameters, was found to give a good description of the peak shapes, and the background was fitted using linear interpolation between 64 points. Representative crystallographic data and refinement residuals at 110, 300, and 800 K are listed in Table 1. Full details for all temperatures are provided in the Supporting Information, SI1.

The 110 K synchrotron powder diffraction data and calculated intensity from the Rietveld model are shown in Figure 2. In addition to the main cubic $CeMnNi_4$ phase (85.6(3) wt %), two impurity phases were refined, namely, hexagonal $CeMnNi_4$ (12.6(2) wt %) and CeO_2 (1.81(3) wt %). The unit cell parameter is shown as a function of temperature in Figure 3. It shows a near linear expansion with expansion coefficients $\alpha_L = 14.7(2) \times 10^{-6}$ K^{-1} (110–300 K) and $\alpha_L = 13.3(2) \times 10^{-6}$ K^{-1} (300–900 K). The origin of the slight systematic error between the low- and the high-temperature data sets is not clear but has a negligible influence on the following discussion about Debye and Einstein temperatures.

Atomic displacement parameters (ADP) are plotted against temperature in Figure 4. It is evident that manganese has larger thermal vibration than both nickel and cerium. This confirms the results of Dhiman et al.[7b] and could suggest that manganese is a rattler located in the cage formed by the cerium and nickel network. However, it should be noted that the absolute values of the ADPs obtained in the present study are approximately

dx.doi.org/10.1021/ic202231k | Inorg. Chem. 2012, 51, 1916–1924

Table 1. Crystallographic Details and Refinement Residuals for $CeMnNi_4$ at Three Different Temperatures[a]

temp./K	110	300	800
exposure time/min	5	5	5
N(data points)	5799	5799	5799
N(reflns)	1696	1706	1743
N(params)	83	83	83
R_{Bragg}	1.28	1.63	4.59
R_F	1.29	1.81	3.94
χ^2	6.80	6.49	8.19
R_p	6.60	7.05	12.8
R_{wp}	8.35	8.44	13.3
a/Å	6.95257(4)	6.96964(5)	7.01447(9)
x_{posn} of Ni	0.62384(3)	0.62388(3)	0.62413(4)
W	0.000766(3)	0.000830(3)	0.000480(4)
X	0.1954(4)	0.2007(5)	0.1871(9)
Y	0.01558(6)	0.01517(6)	0.0187(1)
U_{iso} Ce	0.00338(9)	0.0070(1)	0.0203(3)
U_{iso} Mn	0.0046(2)	0.0096(3)	0.0203(6)
U_{iso} Ni	0.00151(6)	0.00479(8)	0.0150(2)
wt % (cubic $CeMnNi_4$)	85.6(3)	85.4(3)	87.2(5)
wt % (hexagonal $CeMnNi_4$)	12.6(2)	12.8(2)	11.9(3)
wt % (CeO_2)	1.81(3)	1.77(2)	0.93(4)

[a]Data at 300 K are taken from the low-temperature run.

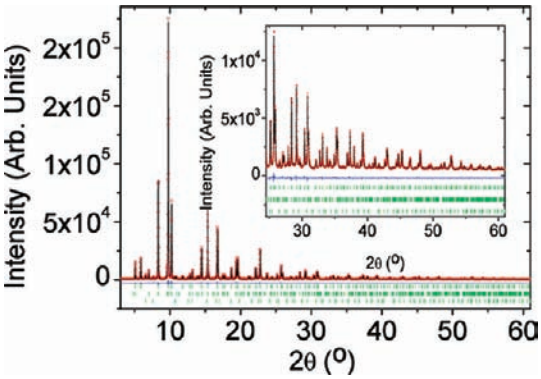

Figure 2. Observed (red), calculated (black), and difference synchrotron X-ray diffraction (blue) patterns for cubic $CeMnNi_4$ at 110 K. Bragg positions of the cubic $CeMnNi_4$ phase are marked with green lines, while impurity phases of hexagonal $CeMnNi_4$ and CeO_2 are the second and third marks, respectively. (Insert) Expansion of the high-angle region.

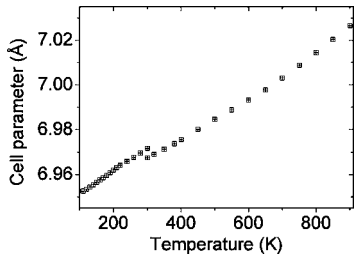

Figure 3. Lattice parameter of cubic $CeMnNi_4$ as a function of temperature.

one-half of the values reported by Dhiman et al. The large void space presumably leads to weak bonding of the Mn atom, and to a first approximation one may assume that Mn behaves like an Einstein oscillator with atomic vibrations that are

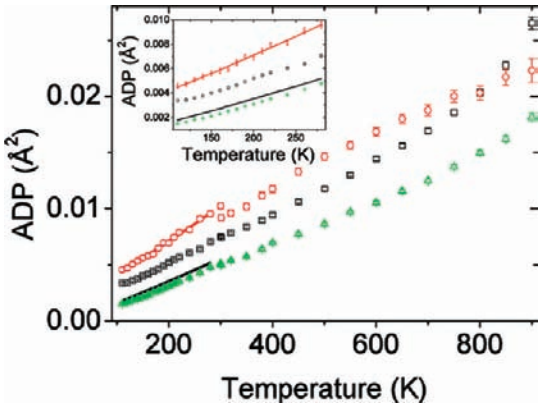

Figure 4. Atomic displacement parameters as a function of temperature with Ce as black squares, Mn as red circles, and Ni as green triangles. Einstein and Debye models have been fitted to the low-temperature data, and the fits are shown as red and black solid lines, respectively. Debye function was fitted to the weighted values of U_{iso}(Ce) and U_{iso}(Ni).

independent of the vibrations of the nickel−cerium network. Similarly, one may approximate that the network behaves as a Debye solid. The ADP data can be used for estimating the Einstein temperature by fitting them to the Einstein expression for ADPs[13]

$$U_{xx}(T) = \frac{\hbar^2}{2mk_B\Theta_{E,xx}}\coth\left(\frac{\Theta_{E,xx}}{2T}\right) + d_{xx}^2$$

where $U_{xx}(T)$ are the anisotropic ADPs, m is the mass of the oscillating atom, Θ_E is the Einstein temperature, and d_{xx}^2 is a disorder term, where a significant nonzero value indicates a temperature-independent, static, or dynamic displacement from the position of the crystallographic model. The Einstein atom is a harmonic oscillator, and the Einstein temperature is directly related to the energy of the vibrational motion of the atom. Similarly, the Debye temperature can be extracted from the ADPs of the host structure atoms by fitting them to the Debye expression[5]

$$U_{iso}(T) = \frac{3\hbar^2 T}{mk_B\Theta_D^2}\left[\frac{T}{\Theta_D}\int_{\Theta_D/T}^{0}\frac{x}{\exp(x)-1}dx + \frac{\Theta_D}{4T}\right] + d^2$$

where $U_{iso}(T)$ is the isotropic ADP, m is the weighted average mass of the Debye oscillators, and Θ_D is the Debye temperature. d^2 is an isotropic, temperature-independent, disorder term analogous to the disorder term in the Einstein expression. x is given by $x = \hbar\omega_D/k_BT$, where ω_D is the Debye frequency ($\Theta_D = \hbar\omega_D/k_B$). A low Debye temperature corresponds to a low velocity of sound in the lattice, which leads to a low lattice thermal conductivity.[14]

The Debye and Einstein fits are shown in Figure 4, and the corresponding Debye and Einstein temperatures are estimated to be 301(2) and 165(2) K, respectively. It is noteworthy that common systematic errors in crystallographic data do not affect the estimates of the Einstein and Debye temperatures very much because they are primarily determined by the shapes of the ADP curves rather than the absolute value. As explained above the ADPs reported by Dhiman et al. based on powder neutron diffraction data are about a factor of two larger than the present values. We tried to estimate Einstein and Debye

dx.doi.org/10.1021/ic202231k | Inorg. Chem. 2012, 51, 1916−1924

temperatures from the ADPs reported by Dhiman et al.,[7b] but it is not possible to obtain reliable values because the ADPs values fluctuate heavily. For Mn the values are 0.010(2) at 17 K, 0.012(2) at 30 K, 0.015(2) at 50 K, 0.011(2) at 70 K, 0.012(2) at 90 K, 0.015(2) at 110 K, 0.010(2) at 130 K, and 0.018(2) at 300 K. It seems that the present synchrotron data are more reliable than the reported powder neutron diffraction data. The Einstein temperature of manganese is high compared to values obtained for well-established rattlers, see Table 2.

Table 2. Einstein Temperatures of Well-Established Rattlers in Clathrates and Skutterudites

compound	rattling atom	Θ_E/K	refs
$Ba_8Ga_{16}Si_{30}$	Ba	69(1)	13
$Ba_8Ga_{16}Ge_{30}$	Ba	62(1)	5a
$Ba_8Al_{16}Ge_{30}$	Ba	61(1)−64(1)	15
$Ba_8In_{16}Ge_{30}$	Ba	57(1)	5b
$Ba_8Zn_{16}Ge_{30}$	Ba	67(1)	16
$Ba_8Cu_{5.9}Ge_{40.1}$	Ba	64(1)	17
$Ba_8Ni_{5.8}Ge_{30.2}$	Ba	79(1)	18
$Sr_8Ga_{16}Ge_{30}$	Sr	∼80	5b
La_xCoSb_3	La	79(3)	9
Eu_xCoSb_3	Eu	68(2)	19
Yb_xCoSb_3	Yb	60(1)	19
Nd_xCoSb_3	Nd	54(4)	19
Sm_xCoSb_3	Sm	70(4)	19
Ce_xCoSb_3	Ce	60(2)	19

The high value of the Einstein temperature of Mn in cubic $CeMnNi_4$ probably means that it cannot hybridize effectively with the acoustic phonons and thereby lead to a lowering of the thermal conductivity. We attempted to measure thermoelectric properties, but during heating the sample cracked and we did not obtain reliable results. If the material is crushed and subsequently pressed using spark plasma sintering a conversion from the cubic to hexagonal polymorph is observed, making characterization of the cubic phase impossible. It is also doubtful if meaningful transport properties can be measured on the present sample, which even before pressing contained 15% impurities.

Specific heat capacity data were measured from 2 to 300 K, and the result is shown in Figure 5. At room temperature the molar heat capacity is ∼148 J/K mol, which corresponds well with the Dulong−Petit value (6·3R) of ∼150 J/K mol. The specific heat capacity can be approximated as a sum of Einstein and Debye oscillators if the electronic contribution is neglected

$$c_v = 9nk_B\left(\frac{T}{\Theta_D}\right)^3\int_0^{\theta_D/T}\frac{x^4e^x dx}{(e^x-1)^2} + 3Nk_B\left(\frac{\varepsilon}{k_BT}\right)^2\frac{e^{\varepsilon/k_BT}}{(e^{\varepsilon/k_BT}-1)^2} + B$$

In this equation the first term is the Debye contribution, the second term is the Einstein contribution, and B is a (small) constant "background" term. n is the number of host structure atoms, Θ_D is the Debye temperature, N is the number of rattlers in the crystal, and $\varepsilon = \hbar\omega_E$. Fitting this equation to the data gives a Debye temperature of 368(2) K and an Einstein temperature of 116(1) K. These values correspond reasonably well with the values of 301(2) and 165(2) K obtained from the ADP data. However, it must be remembered that the sample was impure and consisted of 85.6(3)% cubic $CeMnNi_4$, 12.6(2)% hexagonal $CeMnNi_4$, and 1.81(3) wt % CeO_2. Furthermore, the electronic contribution is neglected from the fit. The ADP data are much less affected by the impurities since their contributions to the diffraction patterns are explicitly modeled in the Rietveld refinements.

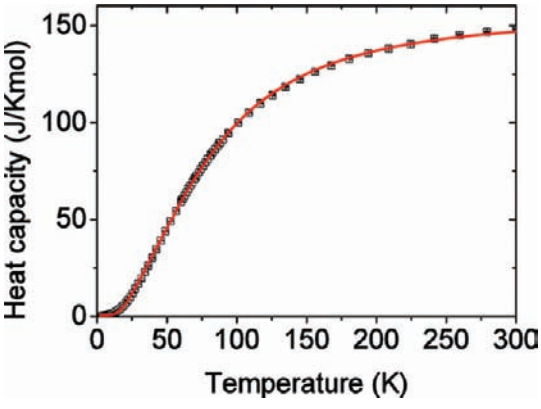

Figure 5. Molar heat capacity as a function of temperature. Solid red line shows the fit obtained from the combined Debye and Einstein model.

Atomic Hirshfeld Surface Analysis. In order to acquire a better understanding of the bonding in $CeMnNi_4$ and especially the potential rattler atom interactions with the host lattice, atomic Hirshfeld surface (AHS) analysis has been undertaken using the program CrystalExplorer.[20] In order to divide the electron density into atomic fragments the Hirshfeld surface approach uses the Stockholder concept.[21] The concept was generalized to extract molecular fragments from a crystal, and a molecular weight function was defined as $w(\mathbf{r}) = \rho_{promolecule}(\mathbf{r})/\rho_{procrystal}(\mathbf{r})$. The promolecule density is a sum of neutral spherically averaged atomic electron density functions centered on the atomic positions for the selected molecular fragment (or atom), whereas the procrystal density is the corresponding density of the surrounding crystal.[22] Spackman and co-workers suggested partitioning space into regions where the promolecule density dominates, i.e., $w(\mathbf{r}) \geq 0.5$. This unique new scheme defines a so-called Hirshfeld surface.[23]

In intermetallic compounds there are usually no well-defined "molecular fragments", and we therefore use atomic Hirshfeld surfaces defined as the region where a particular atomic density dominates over the surrounding procrystal density. This approach provides a tool for analyzing the atomic environment by identifying plausible bonding patterns in nonmolecular crystal structures. In particular, we use the curvedness of the AHS as defined by McKinnon et al.[23b] The present approach was recently introduced to study the interatomic interactions in the hexagonal polymorph of $CeMnNi_4$[24] and $Yb_{14}MnSb_{11}$.[25] However, systematic studies of the ability of the curvedness to study chemical bonding have not been carried out even for molecular systems where the chemical bonding patterns are much simpler to predict. As a test case for the use of AHS to study chemical interaction we included a comparison of the AHS and the topological atoms[26] from the experimental charge density of Co_3(dipyridylamide)$_4Cl_2\cdot nCH_2Cl_2$,[27] in the Supporting Information, see SI2. On the basis of this test case it seems that the AHS resembles the shape of the topological atoms quite well; however, their shapes are more rounded with less distinct features. The curvedness clearly shows the deformation

dx.doi.org/10.1021/ic202231k | Inorg. Chem. 2012, 51, 1916−1924

of the atoms due to bonding, and both high density interactions, covalent bonds, and low-density interactions, ionic character, are visible. Additionally, it is found that the resemblance of the shape is better for the atoms with low integrated charge. This is expected since the AHS are calculated from neutral spherical atomic densities. Overall, it seems that the curvedness is useful for probing atomic interactions. Use of a neutral reference system is both a strength and a weakness of the AHS analysis. Neutral reference systems ensure that the Hirshfeld surfaces are unique and can be compared between different systems. However, as mentioned above, the usability of neutral densities to model highly ionic species may yield erroneous conclusions.

AHS Analysis in Cubic $CeMnNi_4$. The volumes of the Hirshfeld atoms have been calculated for Ce, Mn, and Ni and are listed in Table 3. Due to the larger atomic radii, the Hirshfeld volume of cerium is much larger than the Hirshfeld volumes of both manganese and nickel. The volume of the manganese Hirshfeld atom is significantly larger than that of nickel, even though the atomic radii of the two elements are very similar. This presumably reflects that the manganese atom is positioned in a void, which is larger than what is normally needed for metallic bonding.

Table 3. Atomic Hirshfeld Volumes and Room-Temperature ADPs in $CeMnNi_4$ and $LaCo_4Sb_{12}$

atom	V_{AHS}/Å^3	$ADP_{300\ K}$/Å^2	ADP·m/Å^2·amu
Ce	14.2	0.0070(1)	1.0
Mn	9.3	0.0096(3)	0.5
Ni	7.8	0.00479(8)	0.3
La	19.6	0.018(2)	2.5
Co	7.9	0.00393(7)	0.2
Sb	19.4	0.0055(1)	0.7

It is often a challenge to assign bonding interactions and precise coordination numbers of the atoms in intermetallic compounds. It would therefore be important to have a straightforward tool available to recognize the atomic interactions in intermetallic system and thereby gain a better understanding of the relation between the structure and the properties of a crystal/compound. As indicated in SI1, Supporting Information, and by Skovsen et al.[24] and Kastbjerg et al.,[25] a novel approach to this problem is studying the curvedness of the AHS. Flat regions signify close contacts between the adjacent Hirshfeld atoms, and therefore, such flat regions most likely indicate directional atom−atom interactions. The closer the contact the more deformed the Hirshfeld surface will be. If the real atoms in the solid are not too different from the neutral free atoms used in the AHS calculation (i.e., the electron density distribution is not too different from the free atom electron density) then probably the curvedness also to some extent gives an indication of the strength of the interactions (the closer the contact, the stronger the interactions). However, it should be stressed that the AHS cannot represent absolute "strengths" of chemical bonds (in principle, there are no chemical bonds between free, neutral spherical atoms).

The curvedness mapped on the Hirshfeld surfaces of Ce, Mn, and Ni is shown in Figure 6, and it varies from blue (large curvature) to red regions (flat). The "strength" of the interactions (strong, medium, or weak) can possibly be assigned qualitatively from the curvedness, and an estimate of the coordination numbers of Ce, Mn, and Ni has been given in Table 4, along with the "strength" of the interactions and interatomic distances. The coordination spheres of Ce (turquoise), Mn (yellow), and Ni (red) are shown in Figure 7. Only strong (red bond) and medium (blue bonds) interactions are included. Ce and Mn are shown in similar representation as the corresponding representations in Figure

Table 4. Interatomic Interactions in $CeMnNi_4$ As Defined from the Curvedness of the Atomic Hirshfeld Surfaces[a]

neighbor atom	Ce	Mn	Ni	total
Ce (CN = 16) interatomic distance/Å	0	4(m) 3.021	12(s) 2.895	12(s) + 4 (m)
Mn (CN = 16) interatomic distance/Å	4(m) 3.021	0	12(m) 2.890	16(m)
Ni (CN = 9) interatomic distance/Å	3(m) 2.895	3(w) 2.890	6(s) 2.445	6(s) + 3(m) + 3(w)

[a]Strong curvedness (most negative) is designated as s, m is medium curvedness, and w is weak curvedness.

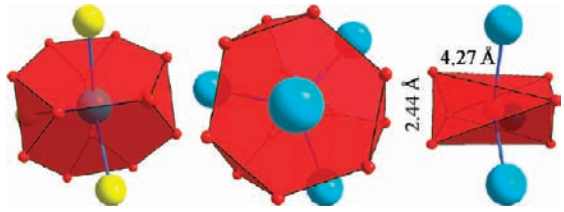

Figure 7. Coordination spheres of Ce (blue), Mn (yellow), and Ni (red). Both Ce and Mn are situated in an octagon consisting of four 3-membered rings and four 6-membered rings of Ni atoms, whereas Ni is located inside an elongated antiprism of Ni.

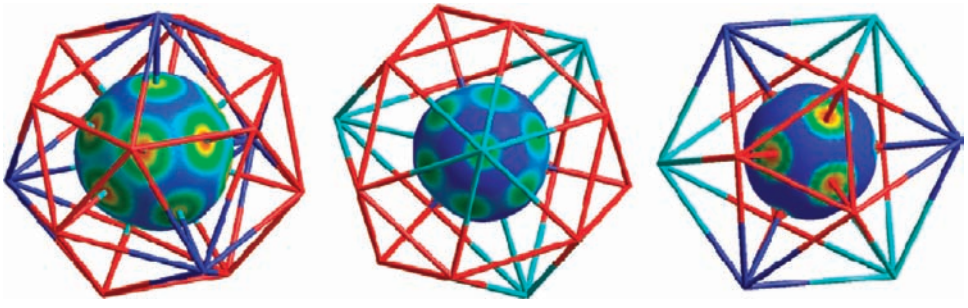

Figure 6. Curvedness plotted on the atomic Hirshfeld surfaces of Ce, Mn, and Ni mapped from −1 (flat; red) to −0.5 (sphere-like; blue). Ce is turquoise, Mn is blue, and Ni is red.

dx.doi.org/10.1021/ic202231k | *Inorg. Chem.* 2012, 51, 1916−1924

Figure 8. (a) Atomic Hirshfeld surfaces of La (white), Co (magenta), and Sb (gray) in the partial La-filled skutterudite $CoSb_3$. (b) Atomic Hirshfeld surface of a Xe atom in $CoSb_3$.

6; however, the representation of Ni has been rotated by 90° in order to show the coordination sphere more clearly. For all three atoms the nearest atoms are Ni, and the corresponding polyhedra are shown. Both Ce and Mn are located inside an octagon with four 3-membered rings and four 6-membered rings. Ce has strong curvedness to Ni, whereas Mn only has medium curvedness toward Ni. The nickel atom has strong curvedness toward its nearest neighbors, and this gives an elongated antiprism coordination. It is of special interest to study the coordination sphere of Mn, as this atom is situated in a relatively large cage and has large ADPs. This presumably is reflected in the AHS analysis, where Mn has a much more spherical AHS than both Ce and Ni, Figure 6; consequently, Mn does not appear to have strong interactions with other atoms. The volume of the Mn and Ni Hirshfeld atoms would be expected to be similar in an ordinary intermetallic compound, but in cubic $CeMnNi_4$ the AHS volume of Mn is significantly larger than that of Ni. An atom in an oversized cage, with longer than normal interatomic distances, is expected to have weaker interactions with the surroundings, and the AHS results therefore confirm expectations. The structural description of manganese in cubic $CeMnNi_4$ seems to fulfill the criteria for what is expected for a "rattler". However, as shown above, the Einstein temperature is found to be rather high (165(1) K) compared with well-established rattlers. Overall, the Mn atom in cubic $CeMnNi_4$ appears to be positioned in an oversized cage-like volume and has large thermal vibration. This is confirmed by the AHS analysis, which shows an almost nondeformed AHS presumably with weak bonding to the Ni–Ce network. Nevertheless, the estimated Einstein temperature is much higher than the values found for rattlers in skutterudites and clathrates. The high Einstein temperature suggests quite strong interactions between Mn and the surrounding "host" structure.

For comparison it may be worthwhile to find out what the AHS analysis shows for the well-established thermoelectric rattler atoms in skutterudites and clathrates. However, in clathrates the rattler atoms always are disordered over several positions and off center in the oversized cage, which adds more complexity.[5b] This makes AHS analysis difficult, and in the following we therefore restrict the analysis to the skutterudites, where the rattler is positioned in the center of the cage without (or at least with very limited) disorder.

AHS Analysis of Rattlers in Skutterudites. The skutterudite $CoSb_3$ partially filled with lanthanum is an archetype of a rattler system,[28] and AHS analysis of selected partially filled skutterudites, $M_{0.1}Co_4Sb_{12}$ (M = La, Ce, Nd, Sm, Eu, and Yb), has been carried out. The crystal structures were derived from Rietveld refinement of high-resolution multitemperature synchrotron powder X-ray diffraction data measured at SPring8, Japan.[19] The program CrystalExplorer[20] cannot generate Hirshfeld surfaces if a site is partially occupied, and the M site was therefore fixed to be fully occupied, something which would be observed in only 10% of the cages. The only parameters used when calculating an AHS are atomic positions and cell parameters, whereas the ADPs of the atoms are not involved. Since the guest atom M has weak interaction with the host-lattice, setting the occupancy to unity should not introduce an error that significantly affects the results. This is corroborated by the fact that the unit cell parameter in $Nd_xCo_4Sb_{12}$ only changes from 9.036(1) for x = 0.02 to 9.041(2) for x = 0.2.[19] Such small changes in unit cell parameters will have very little effect on the calculated AHS.

The curvedness mapped on the AHS of the atoms in $LaCo_4Sb_{12}$ is shown in Figure 8a. In contrast to Mn in $CeMnNi_4$, the La AHS has significant curvedness, which at first sight could indicate significant interactions between the rattling lanthanum atom and the host lattice. The AHSs of Ce, Nd, Sm, Eu, and Yb filler atoms in MCo_4Sb_{12} are very similar to that of $LaCo_4Sb_{12}$, and they are shown in the Supporting Information, see SI3. The significant curvedness of the La AHS in the filled skutterudite seems at variance with the concept of La being weakly bonded to the host lattice and the low Einstein temperature obtained from analysis of the ADPs. However, the La AHS is based on neutral atomic densities, and in reality, the La atom in the skutterudite is expected to be present as a highly charged cation (presumably La^{3+}). As a qualitative approximation of a La^{3+} ion we can use a Xe atom, which has the same

dx.doi.org/10.1021/ic202231k | *Inorg. Chem.* 2012, 51, 1916–1924

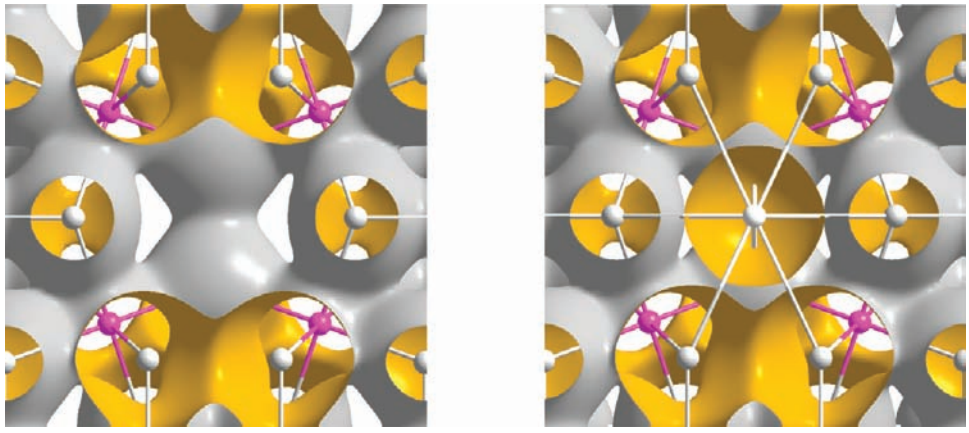

Figure 9. (a) $LaCo_4Sb_{12}$ structure with the La atoms removed, where the void volume is 37% of the unit cell volume. (b) $LaCo_4Sb_{12}$ structure without the La atoms included, where the void volume is 31% of the unit cell volume. Isosurfaces of the procrystal electron density are at 0.024 au (= 0.16 eÅ^{-3}). Gray surface is the inside surface of the void space, and gold surface is the outside surface, that is, the surface toward the atoms. Co atoms are magenta, and Sb atoms are white. La atom, in the center of the right figure, is also white.

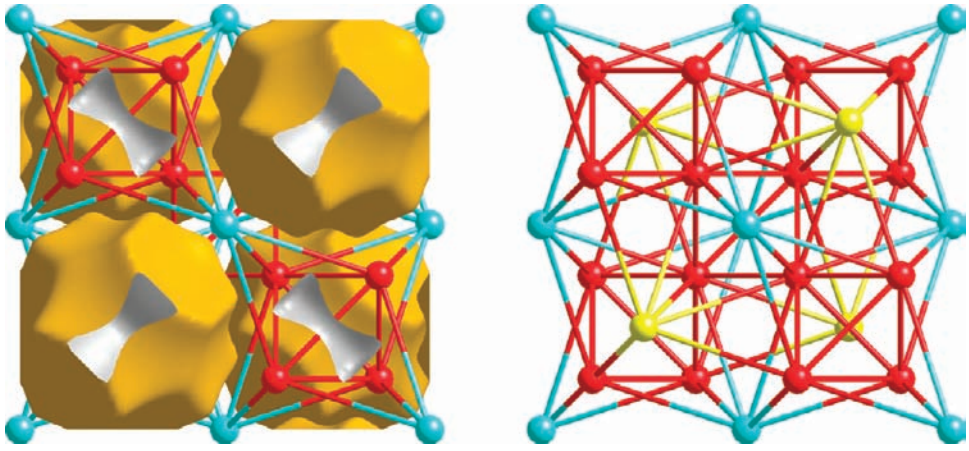

Figure 10. $CeMnNi_4$ structure with the Mn atoms removed. Gray surface is the inside surface of the void space, and gold surface is the outside surface, that is, the surface toward the atoms. Part of the volume around the empty Mn sites protrudes into adjoining unit cells; hence, the appearance of the bow-tie shapes. Void volume is equal to 29% of the unit cell volume. (b) $CeMnNi_4$ structure with the Mn atoms. There is no 0.024 au isosurface when the Mn atoms are included, since 0.024 au is the lowest value of the procrystal electron density in the $CeMnNi_4$ structure. Ce atoms are turquoise, Ni atoms red, and Mn atoms yellow.

electronic configuration but slightly different nuclear charge. The corresponding AHS is shown in Figure 8b. The size and shape of the surface is very different changing from the large and deformed La surface to a small nearly spherical surface of the Xe atom in good correspondence with a weakly interacting rattler atom. The difference in nuclear charge would lead to a slightly smaller radius for the La^{3+} ion than the Xe atom; thus, the interactions would be even weaker than the ones observed here. The positive charge of the La^{3+} ion would be balanced by a negative charge on the framework. At present there is no way of calculating the Hirshfeld surfaces of the negative framework. However, since the occupancy of the La sites is very low (~10%) and the negative charge would presumably be distributed onto the network, the effect on the AHSs would not be as significant as the change of AHS of the cation. In the case of La^{3+} the neutral Xe atom can be used as an isoelectronic substitute; this is not the case for, e.g. Ce, Nd, Sn, Eu, and Yb where the f orbitals are populated. However, since the f electrons are quite localized, the shape of the Hirshfeld surfaces are not greatly affected by the number of f electrons; thus, Xe could potentially be used as a qualitative approximation for the lanthanide series. The approximation would be best for the early lanthanides where the nuclear charge is comparable to Xe and would gradually become worse through the series.

The example above clearly shows the dramatic influence of the diffuse valence electrons on the AHSs. The charge of the Mn atom in $CeMnNi_4$ has been discussed in the literature, and both positive and negative charges have been suggested.[7a,d] In the case of a positive Mn the electrons would likely have been lost from the 4s orbital, thus leading to a smaller less deformed AHS. In contrast, a negative Mn would have a higher population in the 3d orbitals. Since the 3d orbitals are rather localized compared to the 4s orbital the AHS would not be significantly different.

Visualization of Void Spaces. An alternative approach to understand the differences between the nature of the Mn atom in cubic $CeMnNi_4$ and the La atom in $La_{0.1}Co_4Sb_{12}$ is through visualization of isosurfaces of the procrystal electron density. Turner et al. recently demonstrated that this approach can identify and quantify the nature and extent of void space in porous crystalline materials such as metal−organic and covalent−organic frameworks as well as porous and nonporous

dx.doi.org/10.1021/ic202231k | Inorg. Chem. 2012, 51, 1916−1924

molecular crystals.[29] With suitable choice of isovalue it can even be used to identify those intermolecular regions of molecular crystals that change most when subject to external pressure. The isovalues of the procrystal electron density used in that work, 0.002 and 0.0003 au (0.013 and 0.0020 e Å^{-3}, respectively), were appropriate choices for exploring porosity in molecular crystals but are quite inappropriate for the present purposes: the lowest value of the procrystal electron density in the cubic $CeMnNi_4$ structure is 0.024 au (0.16 e Å^{-3}). We therefore choose this isovalue to map the "void" space in unit cells of cubic $CeMnNi_4$ and $LaCo_4Sb_{12}$ (i.e., with the La site fully occupied) and compare that with the "void" space when Mn and La atoms are omitted. For $LaCo_4Sb_{12}$ this isosurface extends throughout the unit cell, comprising 31% of the cell volume, Figure 9. Omitting the La atom increases this volume to 37% of the cell. In contrast, the isosurface is nonexistent for $CeMnNi_4$ (i.e., 0% of the unit cell) and localized to the Mn sites with a total volume of 29% of the unit cell when the Mn atom is omitted from the calculation, Figure 10. It is worth noting that even when the La atom is included in the unit cell there is still much more "empty" space in that structure compared with $CeMnNi_4$ and, in particular, a considerable amount of this space surrounding the La atom. The mapping of void space in the crystal structures documents a clear difference between the excessive void space in the skutterudite structure compared with the tight packing of the $CeMnNi_4$ structure.

In Table 3 we list the ADPs at 300 K and these values multiplied by the atomic masses. In both the Debye and the Einstein models the ADPs are inversely proportional to the mass, and thus, their product presumably is only dependent on temperature. For the Debye atoms the neglect of optical modes in the model is expected to make it increasingly worse with increasing temperature. Furthermore, ADP values obtained from powder diffraction are prone to systematic errors (especially at high temperature), and care should be taken when interpreting absolute values. Nevertheless, for qualitative assessment the product values are still striking. Clearly, the La atom in the skutterudite sticks out with a large value of $\langle u^2\rangle \cdot M$ (2.5), whereas the Mn atom in $CeMnNi_4$ has a value similar to the other atoms (0.5). How about the $\langle u^2\rangle \cdot M$ values for the atoms in thermoelectric clathrates? Literature values for the clathrates are listed in Table 5.

Table 5. Literature $\langle u^2\rangle \cdot M$ Values for the Atoms in Thermoelectric Clathrates[a]

compound	rattler atom	$\langle u^2\rangle \cdot M_{rattler}$	host atoms	$\langle u^2\rangle \cdot M_{host}$	refs
$Ba_8Ga_{16}Ge_{30}$	Ba	4.9	Ga/Ge	0.7	5b
$Sr_8Ga_{16}Ge_{30}$	Sr	9.3	Ga/Ge	1.0	5b
$Eu_8Ga_{16}Ge_{30}$	Eu	20.8	Ga/Ge	0.7	30
$Ba_8Al_{16}Ge_{30}$	Ba	6.0	Al/Ge	0.6	15
$Ba_8Ga_{16}Si_{30}$	Ba	3.5	Ga/Si	0.4	5b
$Ba_8In_{16}Ge_{30}$	Ba	10.5	In/Ge	2.0	5b

[a]For the framework atoms mass-weighted values are used.

For clathrates the $\langle u^2\rangle \cdot M$ values of the rattler atoms is much larger than for La in the skutterudite, but this is due to the fact that the ADP value also contains components from disorder, which is inherent to the clathrate structure. This explains the very large value observed for Eu in $Eu_8Ga_{16}Ge_{30}$, Sr in $Sr_8Ga_{16}Ge_{30}$, and Ba in $Ba_8In_{16}Ge_{30}$. Interestingly, the framework value in $Ba_8In_{16}Ge_{30}$ is also quite large, suggesting that this structure may have significant defects (missing atoms will lead to larger ADP values). The comparison of $\langle u^2\rangle \cdot M$ values corroborates that Mn is not a rattler, whereas the La atom in La_xCoSb_3 and the guest atoms in clathrates have excessive thermal motion.

CONCLUSIONS

Cubic $CeMnNi_4$ has been studied with multitemperature synchrotron powder X-ray diffraction. The previously proposed Mn rattler atom in the structure is found to have relatively large ADP values. However, modeling of the Mn ADPs with the Einstein model leads to an Einstein temperature (Θ_E = 165(2) K), which is much higher than values obtained for well-established rattlers such as guest atoms in skutterudite and clathrates. Atomic Hirshfeld surface (AHS) analysis was carried out on both $CeMnNi_4$ and the archetypical thermoelectric rattler system $LaCo_4Sb_{12}$. The AHS analysis showed that Ce, Mn, and Ni predominantly interact with neighboring Ni atoms. The AHS of the Mn atom shows very little deformation, whereas the AHS of La in $LaCoSb_3$ shows significant deformation. At first sight this could indicate that the Mn atom is weakly bonded to the cage, whereas the La atom in fact is relatively strongly bonded. However, deformation of the La AHS is due to this atom in reality being a cation. Quantification of the void space using the procrystal electron density shows that $CeMnNi_4$ is a condensed structure with a tightly fitting Mn atom, whereas the La atom in $LaCoSb_3$ truly is placed in an oversized void. In addition, the Mn atom in $CeMnNi_4$ has a relatively low $\langle u^2\rangle \cdot M$ value compared with established rattler atoms and a relatively high Einstein temperature. Overall, we conclude that the Mn atom in $CeMnNi_4$ cannot be coined a rattler atom.

ASSOCIATED CONTENT

Supporting Information

This material is available free of charge via the Internet at http://pubs.acs.org.

AUTHOR INFORMATION

Corresponding Author

*E-mail: bo@chem.au.dk.

ACKNOWLEDGMENTS

This work was supported by the Danish National Research Foundation (Center for Materials Crystallography), the Danish Strategic Research Council (Center for Energy Materials), and the Australian Research Council.

REFERENCES

(1) (a) DiSalvo, F. J. *Science* **1999**, *285*, 703−706. (b) Toberer, E. S.; Snyder, G. J. *Nat. Mater.* **2008**, *7*, 105−114. (c) Christensen, M.; Johnsen, S.; Iversen, B. B. *Dalton Trans.* **2010**, *39*, 978−992.

(2) (a) Slack, G. A. *New Materials and Performance Limits for Thermoelectric Cooling*; CRC Press: Boca Raton, FL, 1995. (b) Dresselhaus, M. S.; Chen, G.; Tang, M. Y.; Yang, R. G.; Lee, H.; Wang, D. Z.; Ren, Z. F.; Fleurial, J. P.; Gogna, P. *Adv. Mater. (Weinheim, Germany)* **2007**, *19*, 1043−1053.

(3) (a) Nolas, G. S.; Cohn, J. L.; Slack, G. A.; Schujman, S. B. *Appl. Phys. Lett.* **1998**, *73*, 178−180. (b) Bentien, A.; Palmqvist, A. E. C.; Bryan, J. D.; Latturner, S.; Stucky, G. D.; Furenlid, L.; Iversen, B. B. *Angew. Chem., Int. Ed.* **2000**, *39*, 3613−3616. (c) Keppens, V.; Mandrus, D.; Sales, B. C.; Chakoumakos, B. C.; Dai, P.; Coldea, R.; Maple, M. B.; Gajewski, D. A.; Freeman, E. J.; Bennington, S. *Nature* **1998**, *395*, 876−878. (d) Sales, B. C.; Mandrus, D.; Chakoumakos, B.

C.; Keppens, V.; Thompson, J. R. *Phys. Rev. B* **1997**, *56*, 15081−15089. (e) Iversen, B. B.; Palmqvist, A. E. C.; Cox., D.; Nolas, G.; Stucky, G. D; Blake, N.; Metiu, H. *J. Solid State Chem.* **2000**, *149*, 455−458.
(4) Christensen, M.; Abrahamsen, A. B.; Christensen, N. B.; Juranyi, F.; Andersen, N. H.; Lefmann, K.; Andreasson, J.; Bahl, C. R. H.; Iversen, B. B. *Nat. Mater.* **2008**, *7*, 811−815.
(5) (a) Christensen, M.; Lock, N.; Overgaard, J.; Iversen, B. B. *J. Am. Chem. Soc.* **2006**, *128*, 15657−15665. (b) Bentien, A.; Nishibori, E.; Paschen, S.; Iversen, B. B. *Phys. Rev. B* **2005**, *71*, 144107.
(6) SalesB. C.MandrusD.ChakoumakosB. C.Semiconductors and Semimetals2001
(7) (a) Mazin, I. I. *Phys. Rev. B* **2006**, *73*, 012415. (b) Dhiman, I.; Das, A.; Dhar, S. K.; Raychaudhuri, P.; Singh, S.; Manfrinetti, P. *Solid State Commun.* **2007**, *141*, 160−163. (c) Klimczak, M.; Talik, E.; Kusz, J.; Kowalczyk, A.; Tolinski, T. *Cryst. Res. Technol.* **2007**, *42*, 1348−1351. (d) Murugan, P.; Singh, A. K.; Das, G. P.; Kawazoe, Y. *Appl. Phys. Lett.* **2006**, *89*, 222502.
(8) Murugan, P.; Bahramy, M. S.; Kawazoe, Y. *Phys. Rev. B* **2008**, *77*, 064401.
(9) Mi, J. L.; Christensen, M.; Nishibori, E.; Kuznetsov, V.; Rowe, D. M.; Iversen, B. B. *J. Appl. Phys.* **2010**, *107*, 113507.
(10) (a) Iversen, B. B.; Larsen, F. K.; Figgis, B. N.; Reynolds, P. A.; Schultz, A. J. *Acta Crystallogr., Sect. B* **1996**, *52*, 923−931. (b) Iversen, B. B.; Larsen, F. K.; Pinkerton, A.; Martin, A.; Darovsky, A.; Reynolds, P. A. *Acta Crystallogr., Sect. B* **1999**, *55*, 363−374. (c) Morgenroth, W.; Overgaard, J.; Clausen, H. F.; Svendsen, H.; Jorgensen, M. R. V.; Larsen, F. K.; Iversen, B. B. *J. Appl. Crystallogr.* **2008**, *41*, 846−853.
(11) Nishibori, E.; Takata, M.; Kato, K.; Sakata, M.; Kubota, Y.; Aoyagi, S.; Kuroiwa, Y.; Yamakata, M.; Ikeda, N. *J. Phys. Chem. Solids* **2001**, *62*, 2095−2098.
(12) Rodriguezcarvajal, J. *Physica B* **1993**, *192*, 55−69.
(13) Bentien, A.; Iversen, B. B.; Bryan, J. D.; Stucky, G. D.; Palmqvist, A. E. C.; Schultz, A. J.; Henning, R. W. *J. Appl. Phys.* **2002**, *91*, 5694−5699.
(14) Ascroft, N. W.; Mermin, N. D. *Solid State Physics*; Brooks/Cole: 1976.
(15) Christensen, M.; Iversen, B. B. *Chem. Mater.* **2007**, *19*, 4896−4905.
(16) Christensen, M.; Iversen, B. B. *J. Phys., Condens. Matter* **2008**, *20*, 104244.
(17) Johnsen, S.; Bentien, A.; Madsen, G. K. H.; Nygren, M.; Iversen, B. B. *Chem. Mater.* **2006**, *18*, 4633−4642.
(18) Johnsen, S.; Bentien, A.; Madsen, G. K. H.; Nygren, M.; Iversen, B. B. *Phys. Rev. B* **2007**, *76*, 245126.
(19) Mi, J. L.; Christensen, M.; Nishibori, E.; Iversen, B. B. *Phys. Rev. B* **2011**, *84*, 064114.
(20) Wolff, S. K.; Grimwood, D. J.; McKinnon, J. J.; Jayatilaka, D.; Spackman, M. A. *CrystalExplorer V. 2.0.0 alpha (r367)*; University of Western Australia: Perth, 2011.
(21) Hirshfeld, F. L. *Theor. Chim. Acta* **1977**, *44*, 129−138.
(22) Clementi, E.; Roetti, C. *At. Data Nucl. Data Tables* **1974**, *14*, 177−478.
(23) (a) Spackman, M. A.; Byrom, P. G. *Chem. Phys. Lett.* **1997**, *267*, 215−220. (b) McKinnon, J. J.; Spackman, M. A.; Mitchell, A. S. *Acta Crystallogr., Sect. B* **2004**, *60*, 627−668.
(24) Skovsen, I.; Christensen, M.; Clausen, H. F.; Overgaard, J.; Stiewe, C.; Desgupta, T.; Mueller, E.; Spackman, M. A.; Iversen, B. B. *Inorg. Chem.* **2010**, *49*, 9343−9349.
(25) Kastbjerg, S.; Uvarov, C. A.; Kauzlarich, S. M.; Nishibori, E.; Spackman, M. A.; Iversen, B. B. *Chem. Mater.* **2011**, *23*, 3723−3730.
(26) Bader, R. F. W. *Atoms in molecules: a quantum theory*; Oxford University Press: New York, 1990.
(27) Poulsen, R. D.; Overgaard, J.; Schulman, A.; Ostergaard, C.; Murillo, C. A.; Spackman, M. A.; Iversen, B. B. *J. Am. Chem. Soc.* **2009**, *131*, 7580−7591.
(28) (a) Wang, Y. G.; Xu, X. F.; Yang, J. H. *Phys. Rev. Lett.* **2009**, *102*, 175508. (b) Koza, M. M.; Johnson, M. R.; Viennois, R.; Mutka, H.; Girard, L.; Ravot, D. *Nat. Mater.* **2008**, *7*, 805−810. (c) Ohno, A.; Sasaki, S.; Nishibori, E.; Aoyagi, S.; Sakata, M.; Iversen, B. B. *Phys. Rev. B* **2007**, *76*, 064119.
(29) Turner, M. J.; McKinnon, J. J.; Jayatilaka, D.; Spackman, M. A. *CrystEngComm* **2011**, *13*, 1804−1813.
(30) Paschen, S.; Carrillo-Cabrera, W.; Bentien, A.; Tran, V. H.; Baenitz, M.; Grin, Y.; Steglich, F. *Phys. Rev. B* **2001**, *64*, 214404.